# MULTI-EXCITON STATES IN FLEXIBLE RYDBERG AGGREGATES

A THESIS SUBMITTED TO
THE GRADUATE SCHOOL OF ENGINEERING AND SCIENCE
OF BILKENT UNIVERSITY
IN PARTIAL FULFILLMENT OF THE REQUIREMENTS FOR
THE DEGREE OF
MASTER OF SCIENCE
IN
PHYSICS

By
Ghassan F.M. Abumwis
June 2017

Multi-exciton states in flexible Rydberg aggregates
By Ghassan F.M. Abumwis
June 2017

We certify that we have read this thesis and that in our opinion it is fully adequate, in scope and in quality, as a thesis for the degree of Master of Science.

Sebastian Wüster(Advisor)

Sevilay Sevinçli

Ceyhun Bulutay

Approved for the Graduate School of Engineering and Science:

Ezhan Karaşan
Director of the Graduate School

# ABSTRACT

# MULTI-EXCITON STATES IN FLEXIBLE RYDBERG AGGREGATES

Ghassan F.M. Abumwis
M.S. in Physics
Advisor: Sebastian Wüster
June 2017

Flexible Rydberg aggregates, assemblies of highly excited atoms, provide a platform to investigate quantum phenomena like energy transport and conical intersections. This can be achieved by doping the aggregate with an excitation, an excited state that is energetically higher but close to the primary Rydberg state, which results in the resonant dipole-dipole interaction becoming dominant. Consequently, the excitation is delocalized throughout the aggregate leading to the creation of exciton states.

The properties of excitons have been studied for aggregates with a single excitation only. We follow up on previous results and add a second excitation to the system. Here, we demonstrate that most biexciton states for a dislocated chain at one end, a chain with equal spacing between atoms except for the last two, can be expressed as products of single exciton states. Moreover, we present the atomic trajectories for each biexciton state and we show that non-adiabatic effects are quite prominent in flexible chains of Rydberg atoms. Finally, we analyze the interaction between two excitation pulses based on the initial biexciton state and the presence of a dislocation, then we show some cases where a transmission switch behavior is observable.

Our findings further enhance the range at which flexible Rydberg aggregates can be used to model chemical quantum processes that take place in light harvesting molecules and molecular aggregates. Furthermore, the transmission switch behavior opens the possibility of using Rydberg aggregates in quantum information processing.

*Keywords:* Flexible Rydberg aggregates, excitons, biexciton, non-adiabatic, excitation pulse, dynamics.

# ÖZET

# ESNEK RYDBERG KÜMELERINDE ÇOKLU-UYARIM DURUMLARI

Ghassan F.M. Abumwis
Fizik, Yüksek Lisans
Tez Danışmanı: Sebastian Wüster
June 2017

Esnek Rydberg kümeleri, yani bir arada bulunan yüksek derece uyarılmış atomlar, enerji nakli ve konik kavşaklar gibi kuantum olgularını araştırmak için bir zemin sağlar. Bu, kümenin uyarılarak, enerjisel olarak daha yüksek fakat birincil Rydberg durumuna yakın hale getirilmesi ve rezonant dipol-dipol etkileşiminin egemen hâle getirilmesiyle başarılabilir. Sonuç olarak, uyarma kümenin tamamında delokalize olarak uyarım durumlarının oluşmasına yol açar.

Uyarımların nitelikleri, sadece, tek bir uyarılmanın olduğu kümelerde incelenmiştir. Biz önceki sonuçları takip edip sisteme ikinci bir uyarılma ekledik. Burada, bir ucunda dislokalize olmuş bir zincirde, yani son ikisi hariç atomları arasında eşit uzaklık bulunan bir zincirde, çoğu ikili uyarım durumunun, tek bir uyarım durumlarının ürünleri olarak ifade edilebileceğini göstermekteyiz. Bununla birlikte, her bir ikili uyarım durumu için atomik yörüngeleri sunmakta ve adyabatik olmayan etkilerin Rydberg atomlarının esnek zincirlerinde oldukça öne çıktığını göstermekteyiz. Son olarak, iki uyarılma atışı arasındaki etkileşimi başlangıçtaki ikili uyarım durumu ve dislokalizasyonun varlığına dayanarak inceleyip, iletim değişimi davranışının gözlemlenebilir olduğu birtakım durumları sunduk.

Bulgularımız, ışık hasadı yapan molekül ve molekül kümelerinde gerçekleşen kimyasal kuantum işlemlerinin modellenmesi için esnek Rydberg kümelerinin kullanılabileceği aralığı daha da geliştirmiştir. Bununla birlikte, iletim değişim durumu, Rydberg kümelerinin kuantum bilgi işlemede kullanılması olasılığını ortaya çıkarmıştır.

*Anahtar sözcükler*: Esnek Rydberg kümeleri, uyarım durumları, ikili uyarım, ısıgeçirimsiz olmayan etkilerin, uyarılma atışı, dinamik.

# Acknowledgement

Over the last three years, I had the privilage of studying at Bilkent university. The highlight of my stay was working with Prof. Sebastian Wüster, to whom I express my deepest gratitude. Without his kind guidance this thesis would not have been possible.

I would like to thank my family for their support and patience. A word of thanks goes to Ahmad Hejazy and all of my other friends and colleagues who stood by my side and helped me throughout this whole process.

# Contents

# List of Figures

# Chapter 1

# Introduction

The early 1900's marked the beginning of quantum theory, starting from Planck's solution of black-body radiation [1] followed by Einstein's explanation of the photoelectric effect [2] and Bohr's semi-classical model of the Hydrogen atom in response to the spectroscopic measurements of the spectra of Hydrogen [3]. Henceforth, an intense interest in understanding the underlying physical laws and interactions of atoms led to the discovery of many pure quantum phenomena, one of which is the ability to excite electrons in atoms to a very high principal quantum number or what is called Rydberg atoms.

The excitation process in those days was mainly dependent on electro-mechanical methods, namely "Electron impact excitation" [4] and "Charge exchange excitation" [5]. It was not until the invention of lasers [6] that the true potential of Rydberg atoms could be unlocked [7]. Now armed with the many tools that lasers enabled, scientists throughout the last few decades have been exploring different aspects of those exotic atoms. After the use of laser cooling [8, 9], Rydberg atoms were added to the realm of ultra-cold atomic physics, providing better control over the system and more accurate measurements due to low thermal noise.

The ability to build highly controlled systems of Rydberg atoms along with their long-range interactions made for a perfect modeling device to study some of the fundamental phenomena in physics, including dipole blockade [10], resonant energy transfer [11], mechanical effects of long-range interactions [12, 13], entanglement transport [14, 15], coherent excitation processes [16] and conical intersections [17]. Additionally, a number of applications have been proposed in the fields of quantum optics [18], ultra-cold plasma [19], quantum simulations [20] and quantum information processing [21].

Out of the many proposed applications, we are interested in the effects of dipole-dipole interactions on excitation transport and the motion of Rydberg atoms. For these to exhibit interesting interplay, the system in hand must allow atoms to move freely in at least a one-dimensional configuration and this motion has to be within observable times, in which the system stays in a coherent state and Rydberg states have not decayed. One of the most promising platforms that satisfies these conditions is a flexible Rydberg aggregate [14]. Here, atoms exist in two different Rydberg states making the resonant dipole-dipole interaction dominant over van-der-Waals interaction. This leads to the formation of excitons, states where excitations are delocalized over a number of atoms, and couple the motion of Rydberg atoms to excitation transport [13].

The properties of flexible Rydberg aggregates with one excitation have been examined in a number of studies [13–15, 22, 23]. We build upon these by adding a second excitation to the system and investigate the biexciton states and their dynamics. Specifically, we consider the limits in which biexciton states are reduced to products of single exciton states. We also explore how non-adiabatic processes affect excitation transport and atomic motion. Finally, we study the interaction between single excitation pulses in asymmetric spatial configurations.

These interactions and quantum phenomena are also present in highly complex organic compounds like light harvesting molecules [24]. Unfortunately, the complexity of such systems makes them extremely hard to investigate. On the other hand, the simplicity of Rydberg atoms and their systems give us the ability to study and simulate quantum chemical effects [25, 26].

## 1.1 Thesis outline

In chapter 2, we go through a detailed theoretical description of the characteristics and interactions of Rydberg atoms. We start from a full quantum mechanical treatment of the Hydrogen atom and then generalize the solution, wavefunction and energies, to Alkali atoms and their Rydberg states. Finally, the dipole-dipole interactions between Rydberg atoms are discussed along with the calculations of their dipole matrix element and transition moments.

In chapter 3, we highlight a model to describe the interactions in a flexible Rydberg aggregate with one and two excitations. Later on, we discuss the obtained eigenstates and energies for a number of different one-dimensional configurations.

In chapter 4, building on the model aggregates introduced, we formulate a theoretical description of atomic motion and exciton dynamics. Using Tully's surface hopping algorithm with fewest-switches (FSSH) [27–29], the possibility of non-adiabatic transitions in the system are also considered.

In chapter 5, we reflect on the important results presented and discuss future opportunities for our work.

# Chapter 2

# Rydberg Atoms

The discovery of spectral lines of Hydrogen in the 1880s challenged our understanding of the atomic theory and it was the Swedish physicist Johannes Rydberg who provided an explanation with his famous formula, describing the possible wavelengths of emitted light that result from a "quantum leap" an electron makes between orbitals. He found the formula

$$\frac{1}{\lambda} = R\left(\frac{1}{n_1^2} - \frac{1}{n_2^2}\right), \tag{2.1}$$

where $\lambda$ is the wavelength, $R$ is Rydberg's constant, and $n_1$ and $n_2$ are the principal quantum numbers for the initial and final orbitals that an electron occupies. With few modifications, the formula can be extended to include atoms where the effective nuclear charge is similar to that of Hydrogen. As a result of Rydberg's contributions to the field, atoms with at least one electron excited to a high principal quantum number $n \sim 20...200$ are called Ryberg atoms [30]. The long distance between the nucleus and the excited electron, scaling with $\sim n^2$, leads to a very large dipole moment which in turn makes Rydberg atoms' response to external magnetic and electric fields quite sensitive. Another consequence of this large dipole moment is the dipole-blockade [10] in which a Rydberg atom shifts the energy levels of other neighboring atoms, ones that lie within the blockade radius $\sim \mu m$. If this shift is more than the linewidth of the excitation laser then only one atom is excited in the region. This large interaction range between

Rydberg atoms also leads to strong dipole-dipole coupling that spans over $\mu m$ distances. These properties along with the long lifetime $\sim n^3$ make Rydberg atoms well suited for the study of many fundamental quantum phenomena and their applications.

In this chapter we introduce a detailed theoretical description of Rydberg atoms and their interactions. The analytical solution of the Hydrogen atom and how it can be modified to include Alkali atoms are discussed. Later on, dipole-dipole interactions between two Rydberg atoms are studied.

## 2.1 Hydrogen

Hydrogen is considered the most important reference atom in quantum mechanics. This is mainly due to the fact that its wavefunction and energies can be analytically found, it also can be modified to include Rydberg atoms as the overlap between the excited electron and the positively charged core is small enough to make their description similar to H-atom.

To find the wavefunction and energies we start with the Hamiltonian of Hydrogen

$$\hat{H} = \hat{T} + \hat{V}, \tag{2.2}$$

where $\hat{T}$ is the kinetic energy operator

$$\hat{T} = -\frac{\hbar^2}{2\mu}\nabla^2, \tag{2.3}$$

$\hbar$ is the reduced Planck's constant, $\mu$ is the reduced mass of the electron and $\nabla^2$ is the Laplacian. On the other hand, $\hat{V}$ is the potential energy operator

$$\hat{V} = k_e\frac{e^2}{r}, \tag{2.4}$$

where $k_e$ is Coulomb's constant, $e$ is the electronic charge and $r$ is the distance between the electron and the proton. Then, the Schroedinger equation is

$$\left(-\frac{\hbar^2}{2\mu}\nabla^2 - \frac{k_e e^2}{r}\right)\Psi(r,\theta,\phi) = E\Psi(r,\theta,\phi), \tag{2.5}$$

because the potential does not have an angular dependence which makes it possible to separate the wavefunction into a radial and an angular part, such that

$$\Psi(r, \theta, \phi) = R(r)Y_l^m, \tag{2.6}$$

where $Y_l^m$ are the spherical harmonics defined by azimuthal and magnetic quantum numbers $l$ and $m$ respectively. The solution of the radial part is

$$R(r) = \sqrt{\frac{(n-l-1)!}{2n(n+1)!}\left(\frac{2}{na_o}\right)^3} e^{-\rho/2}\rho^l L_{n-l-1}^{2l+1}(\rho), \tag{2.7}$$

where $L_{n-l-1}^{2l+1}$ are the associated Laguerre polynomials, $n$ as the principal quantum number, $\rho = 2r/na_0$ and $a_o$ is the Bohr's radius. The solution is also a good approximation for Hydrogen-like atoms. The energy is given by

$$E_n = -\frac{13.6}{(n)^2}eV, \tag{2.8}$$

This solution of Hydrogen atom is sufficient to get an idea about the general behavior of the wavefunction and energy levels. However, to get a more accurate picture, a number of additional correction terms must be included in the Hamiltonian, mainly to account for relativistic effects of the movement of electrons around the nucleus, these include spin-orbit coupling, Darwin term, relativistic correction to the kinetic energy term. Thus, the energies can be written as [31]:

$$E_{nj} = -m_e c^2\left(1 - \left(1 + \left(\frac{\alpha}{n - j - \frac{1}{2} + \sqrt{(j+\frac{1}{2})^2 - \alpha^2}}\right)^2\right)^{-1/2}\right), \tag{2.9}$$

where $n$ is the principal quantum number, $j$ is the total angular momentum, and $\alpha$ is the fine structure constant.

There are other corrections that account for the effects of external fields, quantum field theory, nuclear spin and other quantum phenomena. However, they are not of relevance to our work here and thus will not be discussed.

## 2.2 Alkali atoms

The fact that an analytical solution for atoms beside Hydrogen is impossible with our current understanding of the quantum theory, motivates us to use models and approximations that fit experimental results. Especially in the case of Alkali metals, atoms with one valence electron, as their description becomes quite similar to that of Hydrogen when the valance electron is excited to a high $n$ orbit. This is due to the large distance to the core, with an effective charge of $+1$, and the excited electron, which in turn minimizes the overlap with inner shell electrons. However, to get a more accurate description, we must consider the radially-dependent screening effects on the positive charges of the nucleus caused by inner shell electrons. A model potential has been found in agreement with experimental data and is given by [32]

$$V_l(r) = -\frac{Z_l(r)}{r} - \frac{\alpha_c}{2r^4}(1 - e^{-(r/r_c)^6}), \tag{2.10}$$

where $\alpha_c$ is the static dipole polarizability, $r_c$ is a cutoff radius that accounts for the unrealistic contributions of the polarization potential near the origin and $Z_l(r)$ is the radial charge which is defined as

$$Z_l(r) = 1 + (Z-1)e^{-a_1 r} - r(a_3 + a_4 r)e^{-a_2 r}, \tag{2.11}$$

where $Z$ is the nuclear charge and the constants $(a_1, a_2, a_3, a_4, r_c)$ are acquired from a nonlinear fit with the Rydberg energies. These Rydberg energies have been accurately measured for some cases [33, 34] for the alkali atom and $l$ of interest. The spin-orbit coupling undergoes some changes too, making the potential dependent on the total angular momentum $j$ [35]

$$V_{SO}(r) = \frac{\alpha^2}{2r^2}\boldsymbol{L.S}. \tag{2.12}$$

The wavefunctions and energies of the model potential can be found numerically through Numerov's method. However, an analytical formula for the energies can be found from quantum defect theory [36, 37]. Using atomic units, the energies can be written as

$$E_{nlj} = -\frac{R_y}{(n - \delta_{nlj})^2}, \tag{2.13}$$

where $R_y$ is the Rydberg constant and $\delta_{nlj}$ is the quantum defect, which can be written as an expansion

$$\delta_{nlj} = \delta_{lj}^{(0)} + \frac{\delta_{lj}^{(2)}}{(n-\delta_{lj}^{(0)})^2} + \frac{\delta_{lj}^{(4)}}{(n-\delta_{lj}^{(0)})^4} + ... \quad , \tag{2.14}$$

The parameter in 2.14 can be found experimentally through spectroscopy. Some $Li$ quantum defects have been found in [33].

## 2.3 Dipole-dipole interaction

So far, we have discussed the different aspects of a single Rydberg atom. However, much of the exotic properties arise in an ensemble. The many-body problem involving a number of Rydberg atoms can be treated by considering each atom as a dipole with a large dipole moment, a direct result of the large distance between the electron and the positively charged core, consequently making dipole-dipole interaction between atoms dominant. Therefore, we start by calculating the dipole matrix element of a Rydberg atom.

The classical dipole is defined as a pair of equal but opposite charges $q$ placed at a distance $\mathbf{r}$, by changing $\mathbf{r}$ to the distance operator $\hat{\mathbf{r}}$ and $q = e$ we get the quantum mechanical dipole operator for a Rydberg atom

$$\boldsymbol{\mu} = e\hat{\boldsymbol{r}}. \tag{2.15}$$

The dipole matrix between two state $|n, l, m\rangle$ and $|n', l', m'\rangle$ is then $\langle n, l, m|\boldsymbol{\mu}|n', l', m'\rangle$, by rewriting $r$ in the spherical basis

$$\begin{aligned} \boldsymbol{d}_q &= \frac{-q\boldsymbol{e}_x + i\boldsymbol{e}_y}{2}, \quad && q = (-1, 1) \\ &= \boldsymbol{e}_z, && q = 0. \end{aligned}$$

where $e_i$, $i \in (x, y, z)$ is the Cartesian unit vector in the i-direction. Using the Wigner-Eckart theorem [38] and Clebsch-Gordan coefficients $\mathcal{C}^{l,m}_{l',m;1,q}$, this

expression is given by

$$\langle n,l,m|\boldsymbol{\mu}|n',l',m'\rangle = D_{n,l}^{n',l'}\boldsymbol{I}_{l,m'}^{l',m'} \tag{2.16}$$

where $D_{n,l}^{n',l'}$ is the reduced matrix element defined as

$$D_{n,l}^{n',l'} = e\sqrt{\frac{2l'+1}{2l+1}}\mathcal{C}_{l',0;1,0}^{l,0}\langle n,l|\hat{r}|n',l'\rangle \tag{2.17}$$

and

$$\boldsymbol{I}_{l,m'}^{l',m'} = \sum_{q=-1,0,1}\mathcal{C}_{l',0;1,q}^{l,0}\boldsymbol{d}_q. \tag{2.18}$$

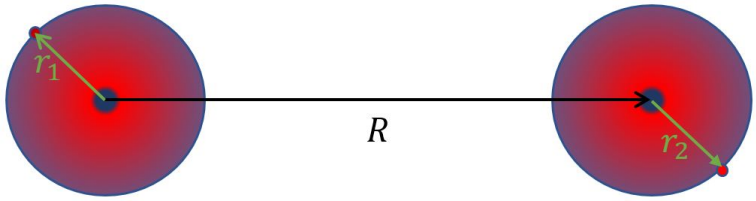


Figure 2.1: A representation of a two atoms system. The electron and the positively charged core are represented by the red dot and blue core respectively.

To find the dipole-dipole forces between two Rydberg atoms placed at a distance $\boldsymbol{R}$ as shown in Fig. 2.1, we start with the potential

$$V = \frac{1}{\boldsymbol{R}} - \frac{1}{|\boldsymbol{R}+\boldsymbol{r}_2|} - \frac{1}{|\boldsymbol{R}-\boldsymbol{r}_1|} + \frac{1}{|\boldsymbol{R}+\boldsymbol{r}_2-\boldsymbol{r}_1|}, \tag{2.19}$$

using the far field approximation and rewriting the potential in terms of $\boldsymbol{\mu}$ we have

$$H_{d-d}(\boldsymbol{R}) = \frac{\boldsymbol{\mu}_1.\boldsymbol{\mu}_2}{R^3} - \frac{3(\boldsymbol{\mu}_1.\boldsymbol{R})(\boldsymbol{\mu}_2.\boldsymbol{R})}{R^5}. \tag{2.20}$$

All matrix elements for the two atoms are

$$M_{ab|a'b'} = \langle n_1l_1m_1|\langle n_2l_2m_2|H_{d-d}|n_1'l_1'm_1'\rangle|n_2'l_2'm_2'\rangle \tag{2.21}$$

where $a$ and $b$ denote a set of indices $(nlm)$ each. As a consequence to symmetry, there will be no permanent dipole moment in the system, thus $M_{ab|ab} = 0 \quad \forall a,b.$

However, if the atoms were in different states e.g. $|ns\rangle$ and $|np\rangle$ then we have a non-zero transition dipole moment $\langle ns|\langle np|H_{d-d}|np\rangle|ns\rangle \neq 0$ which leads to coherent excitation transfer between the two atoms.

One can acquire interaction potentials by diagonalizing 2.20 numerically in a truncated Hilbert space, containing many two-atom Rydberg states in the energetic vicinity of the states of interest. The energies thusly obtained mainly fall into two clear categories, resonant dipole-dipole interaction, which are dominant on large distances and given by

$$E_{Rdd} = -\frac{C_3}{R^3} \tag{2.22}$$

and the short range interaction, which is know as van-der-Waals (VdW)

$$E_{VdW} = -\frac{C_6}{R^6}, \tag{2.23}$$

where $C_3$ and $C_6$ are dispersion coefficients that characterize the strength of both interactions and can be found using the matrix elements. In the special case of using $s$ and $p$ states, $C_3$ is given by

$$C_3 = -\sqrt{\frac{8\pi}{3}}(-1)^{m'}(\langle np|r|ns\rangle)^2 \times \begin{pmatrix} 1 & 1 & 2 \\ m & m' & m'-m \end{pmatrix} Y_{2,m'-m}(\hat{\boldsymbol{R}}) \tag{2.24}$$

where $(...)$ is Wigner 3j coefficient. For a detailed calculation of $C_3$ we refer to [39] and for $C_6$ [40]

## 2.4 Summary

In this chapter Rydberg atoms and their interactions were introduced. Through reflecting on the similarities between Hydrogen and Rydberg atoms, a quantitative description of their energies and wavefunction was found. Then, by treating a Rydberg atoms as dipoles, we were able to calculate the matrix elements which were used to find that coherent excitation transfer is possible between Rydberg atoms. This serves as a foundation to the model presented in the next chapter.

# Chapter 3

# Rydberg aggregates with "multi-excitons"

The exotic properties of Rydberg atoms and their strong interactions, especially the long dipole-dipole interaction, present a promising platform to study different quantum phenomena. Through means of ultracold atomic physics, a small number of Rydberg atoms can be assembled into an aggregate with interatomic distances up to micrometers. These aggregates are made in a highly controlled setup and couple weakly to the environment. They can also be used to study phenomena that are rather difficult to theoretically formulate or experimentally observe in molecular aggregates like coherent energy transfer and exciton dynamics [41].

In this chapter, we introduce a theoretical model to describe the electronic interactions of a one dimensional flexible Rydberg aggregate with one or two excited atoms. This can be experimentally realized by optical trapping which confines atoms to move in one direction. Later on, the electronic eigenstates and their energies are found through numerically solving the electronic Hamiltonian.

## 3.1 Theoretical formulation

We consider a chain of N identical Rydberg atoms that are confined to move in one dimension, the atomic positions are described by $\mathbf{R} = (R_1, R_2, R_3....)$ where $\vec{R_n}$ denotes the position of the $n$th atom and $R_{nm} = |R_m - R_n|$ is the distance between any two atoms. Fig. 3.1. shows a representation of the aggregate.

Figure 3.1: A chain of 5 Rydberg atoms confined to move on one direction with an excitation on the third atom.

Each atom on the chain is initially chosen to be in one of two energetically close Rydberg states, a lower state $|s\rangle$ with energy $\varepsilon_s$ or an excited state "excitation" $|p\rangle$ with $\varepsilon_p$ such that $\varepsilon_p > \varepsilon_s$.

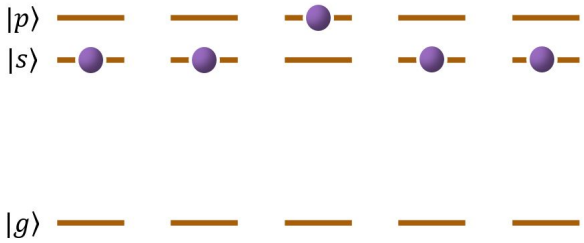


Figure 3.2: An illustration of $|\pi_3\rangle$ state for a chain of 5 Rydberg atoms. $|g\rangle$ here represents the ground state of the considered atom.

### 3.1.1 Single exciton Hamiltonian

We denote the many-body state of a chain with a single excitation $p$ on the $nth$ atom by

$$|\pi_n\rangle = |s..p..s\rangle\,, \tag{3.1}$$

The single excitation states defined in equation 3.1 and illustrated in Fig. 3.2

span a basis in which the total Hamiltonian can be written as

$$\mathcal{H}(\mathbf{R}) = -\sum_{n=1}^{N} \frac{\nabla^2_{R_n}}{2M} + \mathcal{H}^{el}(\mathbf{R}). \tag{3.2}$$

$H^{el}$ is the electronic Hamiltonian which is defined in terms of $H^{dd}$ "the dipole-dipole interaction" and $H^{VdW}$ "the van-der-Waals interaction" such that

$$\mathcal{H}^{el}(\mathbf{R}) = H^{dd} + H^{VdW}, \tag{3.3}$$

where

$$H^{dd}(\mathbf{R}) = \sum_{n,m:n\neq m}^{N} \frac{\mu^2}{R^3_{nm}} |\pi_n\rangle \langle\pi_m| . \tag{3.4}$$

The isotropic expression in equation 3.4 can be acquired by a smart selection of states where orientation effects can be ignored [14]. Here, $\mu$ is the transition dipole moment between $|s\rangle$ and $|p\rangle$ as defined in chapter 2.

$H^{VdW}$ is the off-resonant van-der-Waals coupling which can be neglected for large inter-atomic distances. However, as atoms get closer to each other, it becomes more significant, especially when simulating the dynamics as it works as a stopping mechanism to prevent collisions

$$H^{VdW}(\mathbf{R}) = E_0 + \sum_{n}^{N} E_n(\mathbf{R}) |\pi_n\rangle \langle\pi_n| , \tag{3.5}$$

with

$$E_n(\mathbf{R}) = -\sum_{l,k:l\neq k}^{N} \frac{C_6^{ss}}{2R^6_{lk}} - \sum_{l\neq n}^{N} \frac{C_6^{ps} - C_6^{ss}}{2R^6_{ln}}. \tag{3.6}$$

Because van-der-Waals interaction plays a practical role here, we set $E_0$ to be zero. Moreover, we choose $C_6 = C_6^{ss} = C_6^{ps}$ and $C_6 < 0$ to make sure that the interactions are repulsive. Thus,

$$E_n(\mathbf{R}) = -\sum_{l,k:l\neq k}^{N} \frac{C_6}{2R^6_{lk}}. \tag{3.7}$$

Finally, the complete electronic Hamiltonian of the system is

$$\mathcal{H}_1^{el}(\mathbf{R}) = \sum_{n,m:n\neq m}^{N} \frac{\mu^2}{R_{nm}^3} |\pi_n\rangle \langle\pi_m| - \sum_{n}^{N} \sum_{l,k:l\neq k}^{N} \frac{C_6}{2R_{lk}^6} |\pi_n\rangle \langle\pi_n| . \tag{3.8}$$

### 3.1.2 Biexciton Hamiltonian

In this part, we consider a chain of N atoms with 2 excitations where both cannot exist on the same atom nor can they transport to different locations at the same time. Then, let us assume that $\mathcal{A} = \{\Pi_1, .., \Pi_i, ..\Pi_{\bar{N}}\}$ is the set of all combinations of possible atomic positions $n_i, m_i$ that excitations can occupy, such that $\Pi_1 = \{1, 2\}$, $\Pi_2 = \{1, 3\}$ and so on, with $\bar{N} = \binom{N}{2}$ as the total number of combinations. Thus, a Hilbert space can be constructed by assigning each combination $\Pi_i$ to a basis

$$|\Pi_i\rangle = |n_i m_i\rangle = |s..p..p..s\rangle , \tag{3.9}$$

where both atoms $n_i$ and $m_i$ are in the p-state while other atoms are in s-state. This can be used to write the electronic Hamiltonian

$$\mathcal{H}_2^{el}(\mathbf{R}) = \sum_{i,j:i\neq j}^{\bar{N}} V_{ij}(\mathbf{R}) |\Pi_i\rangle \langle\Pi_j| - \sum_{i}^{\bar{N}} |\Pi_i\rangle \langle\Pi_i| \sum_{l,k:l\neq k}^{N} \frac{C_6}{2R_{lk}^6}, \tag{3.10}$$

where $\bar{N} = \binom{N}{2}$ and,

$$V_{ij}(\mathbf{R}) = \left( \delta_{m_i m_j} \frac{\mu^2}{R_{n_i n_j}^3} + \delta_{n_i n_j} \frac{\mu^2}{R_{m_i m_j}^3} + \delta_{m_i n_j} \frac{\mu^2}{R_{n_i m_j}^3} + \delta_{n_i m_j} \frac{\mu^2}{R_{m_i n_j}^3} \right). \tag{3.11}$$

## 3.2 Results

In this section, we present the numerical solution for the eigenvalue problem of both the single exciton and the biexciton electronic Hamiltonians.

For the single exciton case

$$H_1^{el}\phi_k^N(\mathbf{R}) = U_k\phi_k^N(\mathbf{R}), \tag{3.12}$$

where $U_k$ are the energies which define BO surfaces and $\phi_k^N$ are the eigenstates for a chain of $N$ atoms, called Frenkel excitons [42]. The set of $\phi_k^N(\mathbf{R})$ vectors form an adiabatic basis to which we can expand the total wavefunction $\Psi^{(i)}$, The superscript refers to the number of excitations in the chain.

$$\Psi^{(1)} = \sum_k^N c_k(t)\phi_k^N(\mathbf{R}) \tag{3.13}$$

and for the biexciton case we have

$$H_2^{el}\zeta_k^N(\mathbf{R}) = O_k\zeta_k^N(\mathbf{R}), \tag{3.14}$$

where $O_k$ are the energies and $\zeta_k^N$ are the eigenstates and the total wavefunction is

$$\Psi^{(2)} = \sum_k^{\bar{N}} \alpha_k(t)\zeta_k^N(\mathbf{R}), \tag{3.15}$$

where $c_k$ and $\alpha_k$ the probability amplitudes for finding the system in the $kth$ state

In our numerical simulations, $^7$Li has been used as a specimen with an atomic mass of M=11000 a.u, a transition dipole moment $\mu$=1000 a.u. corresponding to n $\approx$ 40 and $C_6 = -8.571 \times 10^{18}$. Later on, the adiabatic eigenstates and their respective energies are found for two distinctive configurations:

1. Regular chain with equal distance between neighboring atoms set at $R = 5\mu m$, as shown in Fig. 3.1

2. Dislocated chain at one end, where the last atom on one end of the chain is brought to $\frac{R}{2}$ of its neighboring atom.

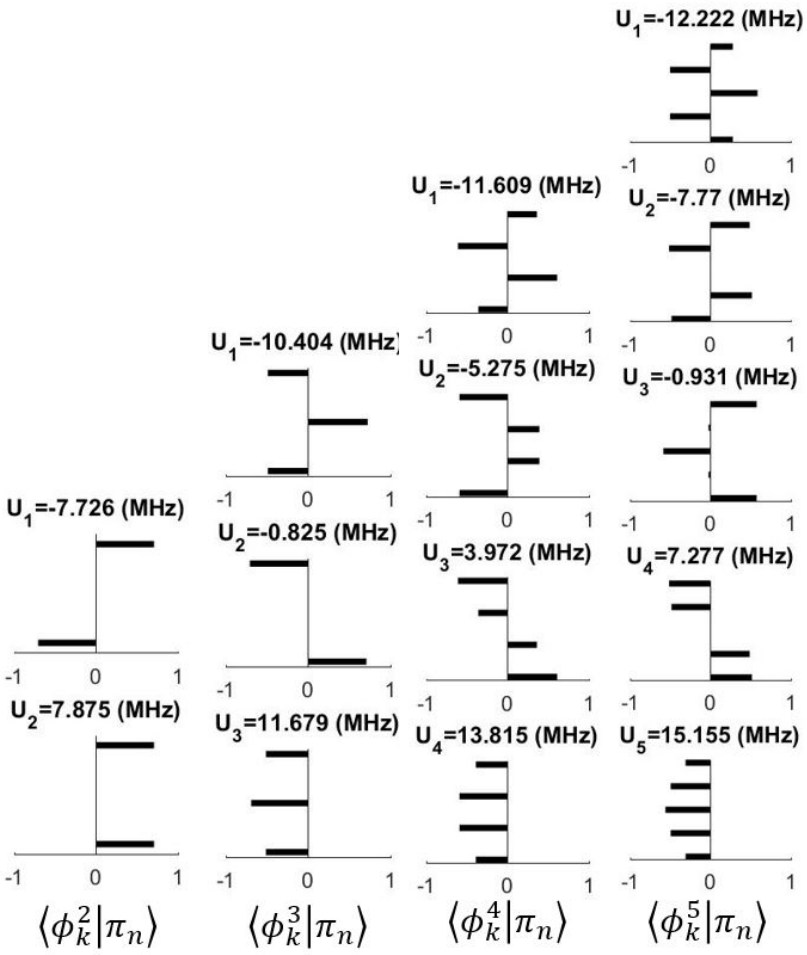


Figure 3.3: The electronic eigenstates for a regular chain of 2,3,4,5 atoms (a,b,c,d) respectively, the horizontal bars represent the probability amplitude of finding the excitation on $nth$ atom for the $kth$ state. With $U_k$ as the energy of the eigenstate.

### 3.2.1 Single exciton states

The probability amplitudes of finding an excitation on a certain atom are given by $\langle \phi_k^N | \pi_n \rangle$, which not only allows to find the probability but also determines the direction of the initial forces between atoms. We will discuss this in more details in chapter 4. Fig. 3.3 shows a representation of these probability amplitudes for a regular chain of 2,3,4 and 5 atoms for all $k's$. Our results for the latter agree with [13] and hence verify our codes. We notice that, the excitation is spread over the whole chain with each atom carrying a fraction of it.

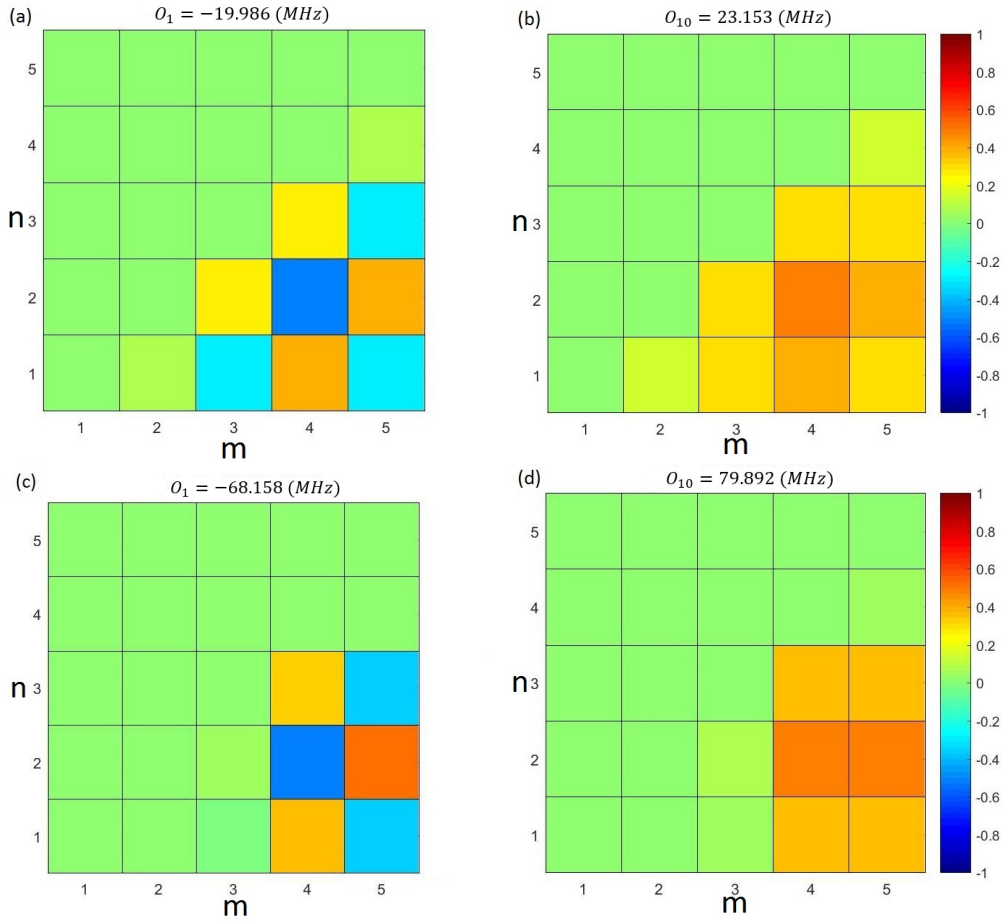


Figure 3.4: The electronic eigenstates for two excitations $\zeta_1^5$ and $\zeta_{10}^5$ for both a regular chain (a),(b) and a chain with a dislocation at one end (c),(d). With $n, m$ representing the atomic locations of the first and second excitation respectively, which follows form the convention used in 3.16.

### 3.2.2 Biexciton states

After showing the simple single exciton case, mainly for verification, we proceed to examine the biexciton results. The probability amplitudes of finding an excitation on atom $n$ while the other excitation is on atom $m$ can be found using

$$P_{nm} = \left\langle nm \middle| \zeta_k^N \right\rangle, \tag{3.16}$$

The electronic eigenstates of a regular chain $\zeta_1^5$ and $\zeta_{10}^5$ shown in Fig. 3.4 (a) and (b) are the ones with the highest attractive and repulsive potentials. This results in the de-localization of both excitations throughout the whole chain. On the

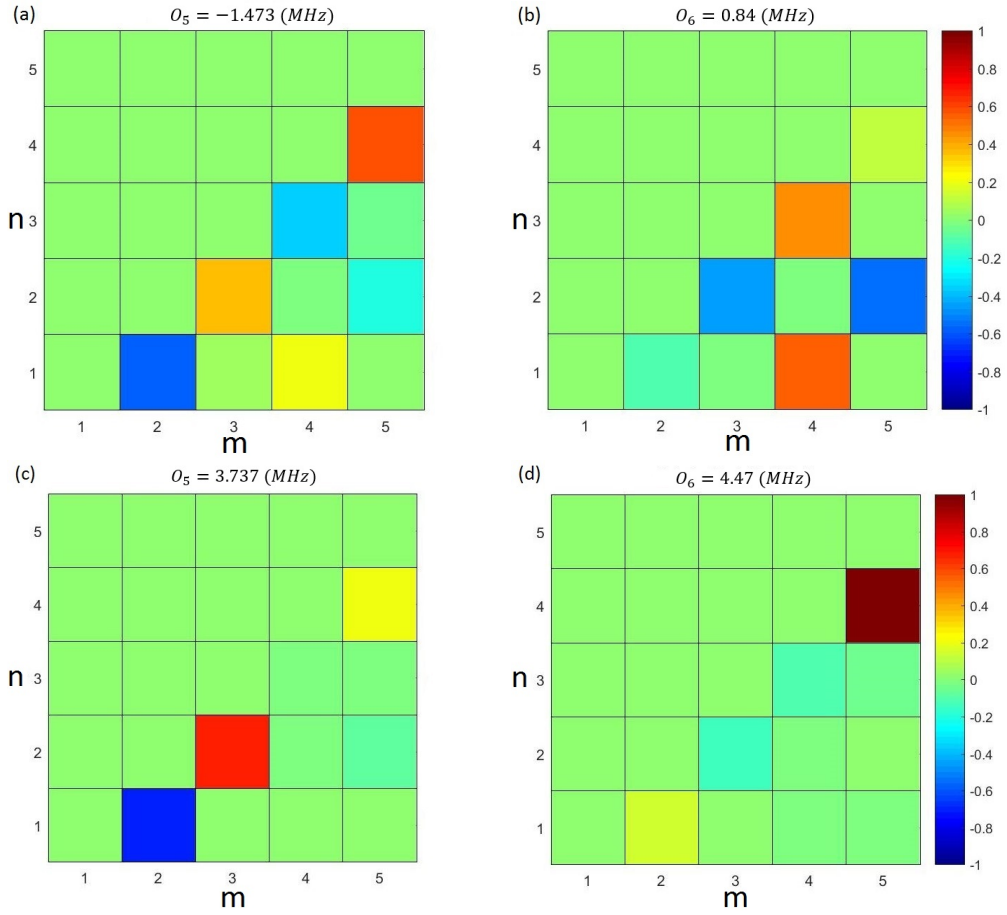


Figure 3.5: The electronic eigenstates $\zeta_5^5$ and $\zeta_6^5$ for both a regular chain (a),(b) and a chain with a dislocation at one end (c),(d). With $n, m$ representing the atomic locations of the first and second excitation, respectively.

other hand, In Fig. 3.4 (c) and (d) the same states are shown for a dislocated chain at one end. Having this dislocation, increases the coupling strength between the dislocated atoms, in this case the 4th and 5th atoms, which in turn eliminates the de-localization of both excitations, showing that one excitation is localized on the dislocated end of the chain while the second excitation is localized on the other three atoms.

We also notice that the 10th case for both configurations has the excitations in phase, that is all amplitudes on each atom are positive, while for the 1st cases the excitations are out of phase as their probability amplitudes have alternating signs.

Fig. 3.5 (a) and (b) shows the weakest attractive and repulsive states of a regular

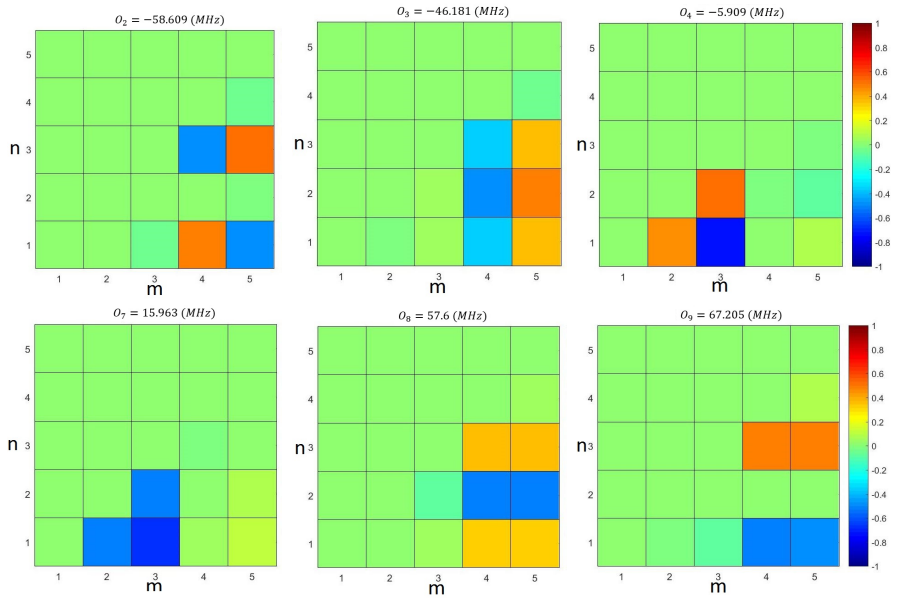


Figure 3.6: The electronic eigenstates $\zeta^5_{2,3,4,7,8,9}$ of a chain with a dislocation at one end, with $n, m$ representing the atomic locations of the first and second excitation, respectively.

chain respectively. We notice a sparse spread of possible excitonic locations, mainly with the excitations localized on neighboring atoms or two locations apart namely (1,4) and (2,5). In Fig. 3.5 (c) and (d) are the same states for a dislocated chain. We notice that the exciton localization is further enhanced with only the neighboring states becoming available. Interestingly, it also shifts the energy of $\zeta^5_5$ to make it repulsive.

Adding a dislocation also helps with characterizing the electronic states. For the $N = 5$ case Fig. 3.6 shows the other six states of the dislocated chain we previously introduced. Now, with a total of 10 states, we notice that six of them ($\zeta^5_1,\ \zeta^5_2,\ \zeta^5_3,\ \zeta^5_8,\ \zeta^5_9,\ \zeta^5_{10}$) can be understood as the product of states from two separate chains each with a single exciton on it. Specifically, one chain with the two atoms at the dislocation $|sp\rangle$ and another with the remainder three atoms $|ssp\rangle$. Such that

$$\zeta^5_1 \sim \phi^2_1\phi^3_1 \tag{3.17a}$$

$$\zeta^5_2 \sim \phi^2_1\phi^3_2 \tag{3.17b}$$

$$\zeta^5_3 \sim \phi^2_1\phi^3_3 \tag{3.17c}$$

$$\zeta_8^5 \sim \phi_2^2\phi_1^3 \tag{3.17d}$$

$$\zeta_9^5 \sim \phi_2^2\phi_2^3 \tag{3.17e}$$

$$\zeta_{10}^5 \sim \phi_2^2\phi_3^3, \tag{3.17f}$$

where the first $\phi^2$ state describes excitation on atom $1-2$ and the second $\phi^3$ on atom 3-5. Moreover, ($\zeta_4^5$, $\zeta_5^5$, $\zeta_7^5$) can be explained as if both excitations were on a regular chain of 3 atoms $|pps\rangle$ which, due to the interchangeability of $s$ and $p$, is equivalent to the state $|pss\rangle$. Where,

$$\zeta_4^5 \sim \phi_1^3\phi_0^2 \tag{3.18a}$$

$$\zeta_5^5 \sim \phi_2^3\phi_0^2 \tag{3.18b}$$

$$\zeta_7^5 \sim \phi_3^3\phi_0^2 \tag{3.18c}$$

Lastly.

$$\zeta_6^5 \sim \zeta_0^2\phi_0^3, \tag{3.19}$$

where $\zeta_0^2 = |pp\rangle$, $\phi_0^3 = |ss\rangle$ and $\phi_0^2 = |sss\rangle$. The superscript indicates the number of atoms in the chain.

## 3.3 Conclusion

We have first studied the exciton states induced by dipole-dipole and van-der-Waals interactions in a static Rydberg aggregate. We found that excitations on a regular chain would be shared among atoms. However, introducing a dislocation at one end limits the delocalization to a selected number of atoms, in which case the dislocated Rydberg chain could be understood in terms of two separate chains with each holding a single exciton.

The model introduced in this chapter presents a description for an experimentally feasible setup, where the properties of a Rydberg aggregate could be investigated. Furthermore, it lays a foundation for studying exciton transfer and the motion of trapped atoms which will be discussed in the next chapter.

# Chapter 4

# Flexible Rydberg aggregates with multiple excitations

The dynamics of unfrozen systems, ones in which constituents are not bound by an external potential, are induced by interactions between its elements. Flexible Rydberg aggregates are an example of such a system where the strong dipole-dipole interaction is the main drive for atomic motion. Consequently, the coupling between spatial degrees of freedom, eigenstates and energies results in the emergence of many interesting properties such as coherent excitation transport. It also has been shown that the coherent splitting of an exciton pulse is possible through conical intersections (Cl) in a Rydberg aggregate [23, 43]. This plays a crucial role in many quantum chemical processes where they enable highly non-adiabatic dynamics on an ultrafast time scale [44].

In this chapter, we introduce a theoretical formulation to study exciton dynamics of a flexible Rydberg chain that is confined to move in one dimension. Later on, we study the motion and exciton properties for a chain with one and two excitations, taking into consideration non-adiabatic processes. Finally, we present our numerical results for the trajectories and excitation density of the chain.

## 4.1 Theoretical Formulation

The dipole-dipole induced motion of atoms in the aggregate can be studied by solving the time-dependent Schroedinger equation

$$i\hbar\frac{\partial}{\partial t}\Psi(\mathbf{R},t) = \mathcal{H}\Psi(\mathbf{R},t), \tag{4.1}$$

where $\mathcal{H}$ is the total Hamiltonian and $\Psi(\mathbf{R},t)$ is the wavefunction. By substituting the wave function of the single exciton case equation 3.13 in 4.1 and assuming that atomic motion follows classical trajectories while that of electrons is quantum, we end up with $N$ coupled differential equations of the probability amplitudes $c_k$

$$i\hbar\dot{c}_k = U_k c_k - i\hbar\sum_{i=1}^{N}(\dot{\mathbf{R}}.\mathbf{d}^1_{ki})c_i, \tag{4.2}$$

where $\mathbf{d}^N_{ki}$ is the "non-adiabatic coupling vector" defined as $\mathbf{d}^1_{ki} = \left\langle \phi^N_k \middle| \boldsymbol{\nabla}_R \phi^N_i \right\rangle$ which can be rewritten using the Hellmann-Feynman theorem as

$$\mathbf{d}^1_{ki} = \frac{\left\langle \phi^N_k \middle| \boldsymbol{\nabla}\mathcal{H}^{el}_1(\mathbf{R}) \middle| \phi^N_i \right\rangle}{U_i(\mathbf{R}) - U_k(\mathbf{R})}, \tag{4.3}$$

such that $k \neq i$ and $\mathbf{d}^1_{kk} = 0$.

$\mathbf{d}^1_{ki}$ becomes more significant as potential energy (BO) surfaces become degenerate, forming what is known as a conical intersection. Near these the BO approximation breaks down, allowing for non-adiabatic jumps between BO surfaces. Thus, in order to account for these jumps, we use Tully's surface hopping with fewest switches [27, 29]. In Tully's surface hopping, a mixed quantum-classical method is used, where the excitation dynamics are fully simulated in quantum mechanics while the nuclear trajectories are obtained from the classical equations of motion

$$\mathbf{F}_1 = M\ddot{\mathbf{R}} = -\boldsymbol{\nabla}_{\mathbf{R}} U_{\gamma_1(t)}(\mathbf{R}), \tag{4.4}$$

where $\gamma(t)$ is an index that describes to which BO surface the system belongs, as it evolves in time.

Following a similar approach for the biexciton case and by substituting the wave

function 3.15 in 4.1 we have

$$i\hbar\dot{\alpha}_k = O_k\alpha_k - i\hbar\sum_{i=1}^{\bar{N}}\alpha_i(\dot{\mathbf{R}}.\mathbf{d}_{ki}^2), \tag{4.5}$$

with

$$\mathbf{d}_{ki}^2 = \frac{\left\langle\zeta_k^N\middle|\boldsymbol{\nabla}\mathcal{H}_2^{el}(\mathbf{R})\middle|\zeta_i^N\right\rangle}{O_i(\mathbf{R}) - O_k(\mathbf{R})}, \tag{4.6}$$

and

$$\mathbf{F}_2 = M\ddot{\mathbf{R}} = -\boldsymbol{\nabla}_{\mathbf{R}}O_{\gamma_2(t)}(\mathbf{R}). \tag{4.7}$$

## 4.2 Results

The numerical simulations presented in this section are done using the same parameters as in chapter 3. The trajectories of a chain with a single excitation are presented in the first section, while in the second we present the trajectories with the consideration of possible non-adiabatic jumps between states.

### 4.2.1 Single exciton dynamics

The trajectories of a regular chain of five atoms are shown in the right column of Fig. 4.1 with the corresponding initial states on the left. We notice that the motion of atoms is symmetric around the center of mass, where a pair of atoms experiences a repulsive force if the sign of the probability amplitudes on the respective locations is the same, otherwise the force is attractive. This agrees with [13] and that makes us confident that the non-trivial implementation of Tully's algorithm was successful. However, it agrees when VdW is not considered and $\mu < 0$, benchmarking the code.

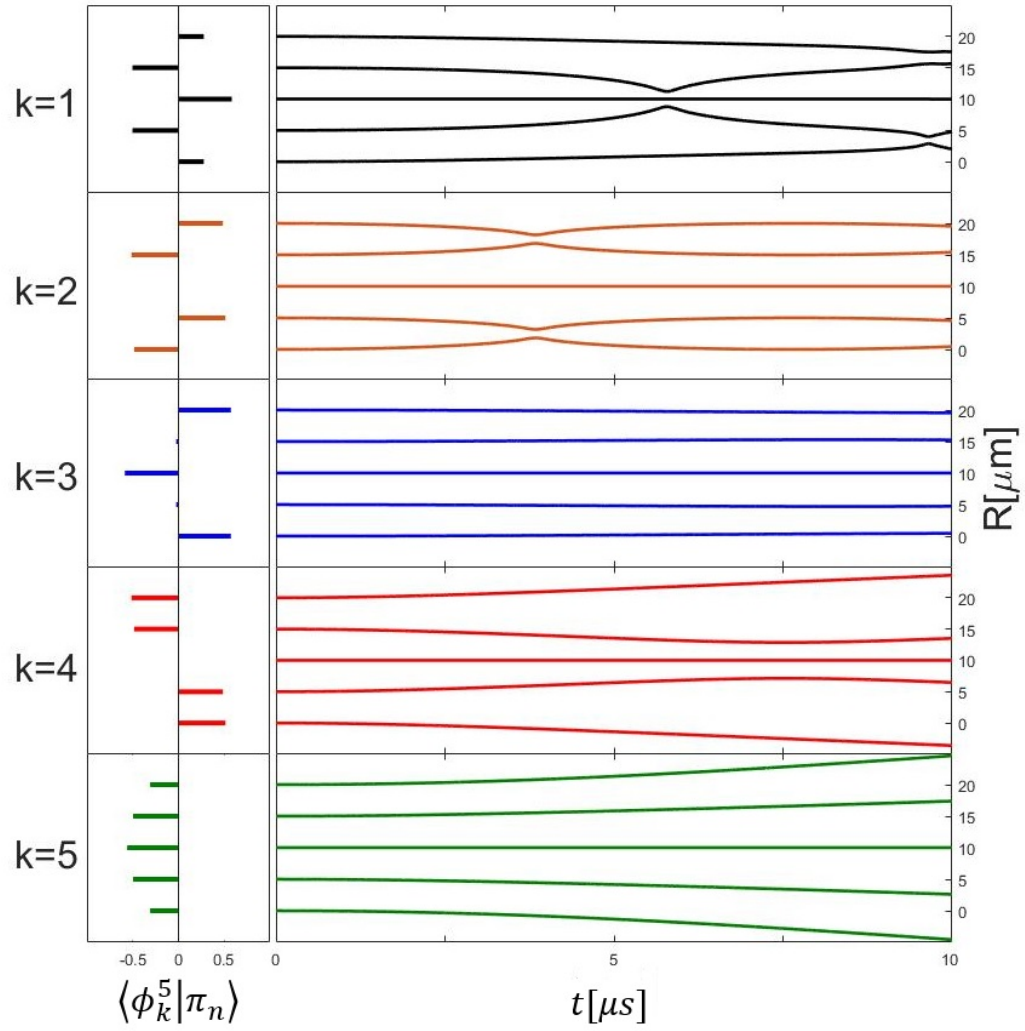


Figure 4.1: The initial electronic eigenvectors of a regular chain with five atoms "left side" and the atomic trajectories "right side", when the system is prepared in the respective eigenvector on the left side.

### 4.2.2 Biexciton dynamics

We start with introducing single trajectories of a regular chain of five atoms with two excitations are shown in the right column of Fig. 4.2 and in Fig. 4.3 with the corresponding initial states on the left. We notice that the motion of atoms follow the same rules as of the single excitation case.

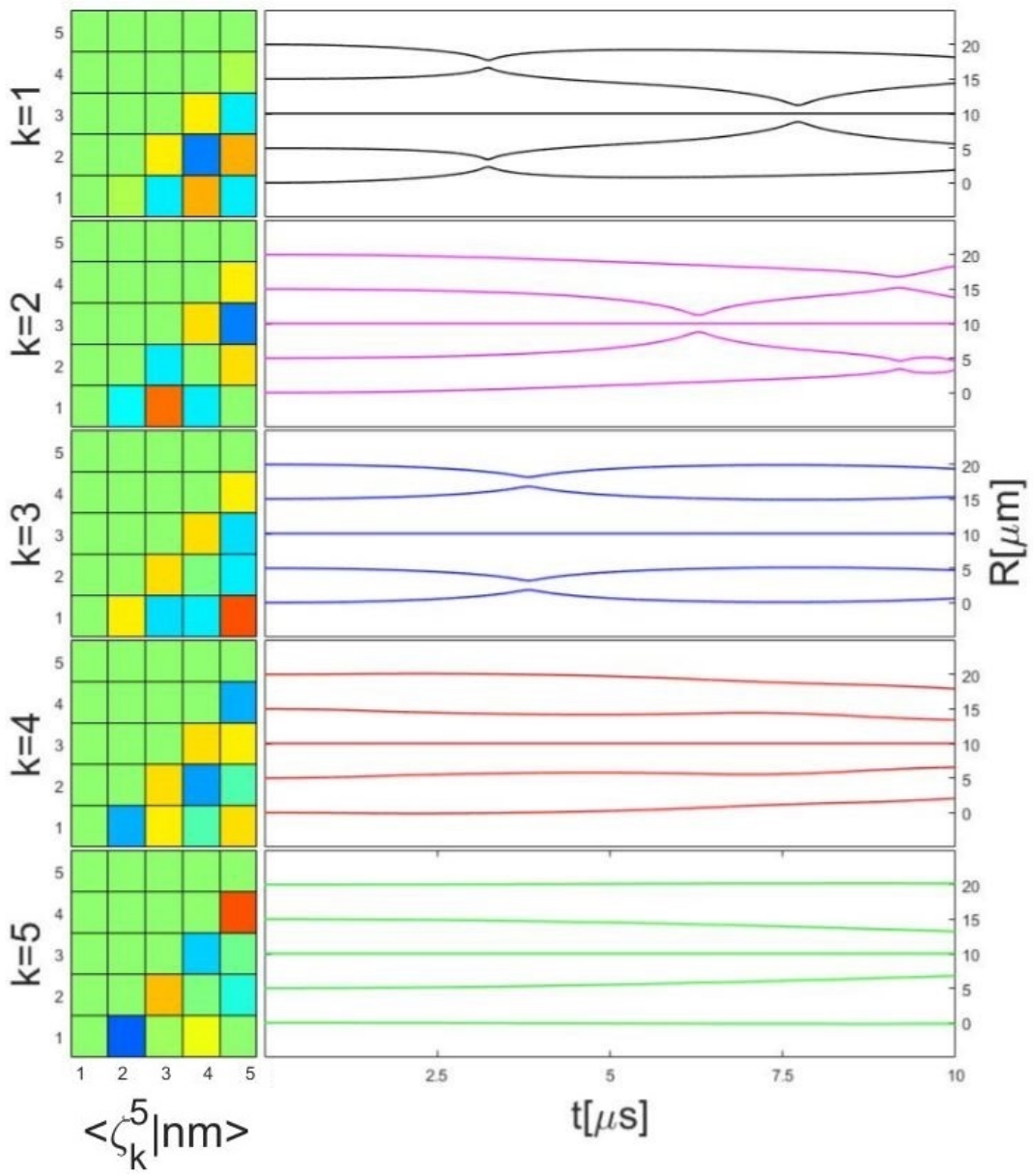


Figure 4.2: The electronic eigenvectors 1-5 of a regular chain of five atoms with two excitations "left side" and the atomic trajectories "right side", when the system is prepared in the respective eigenvector on the left side. The colors on the left side follow the same color pattern as of Fig. 3.6

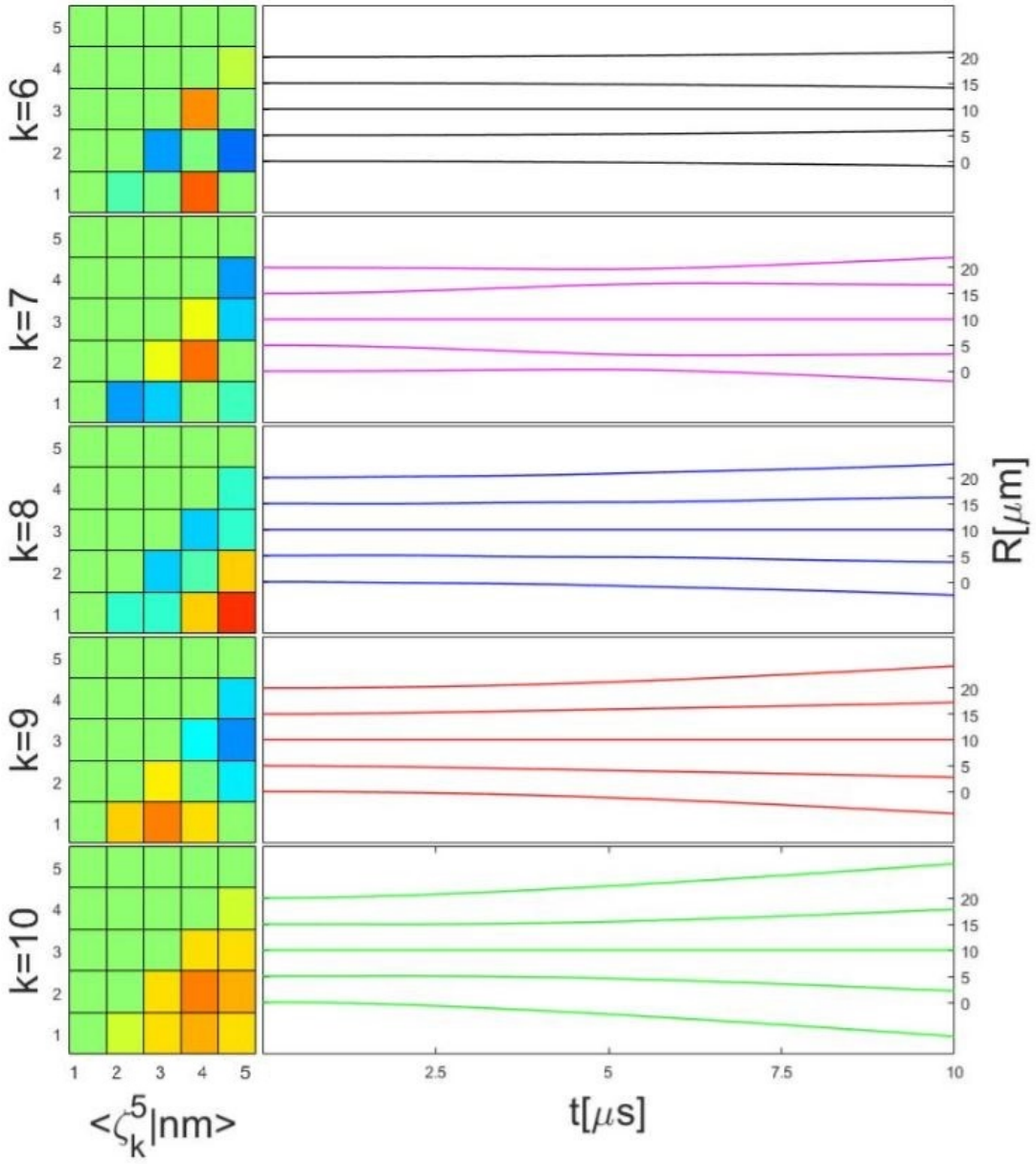


Figure 4.3: The electronic eigenvectors 6-10 of a regular chain of five atoms with two excitations "left side" and the atomic trajectories "right side", when the system is prepared in the respective eigenvector on the left side. The colors on the left side follow the same color pattern as of Fig. 3.6

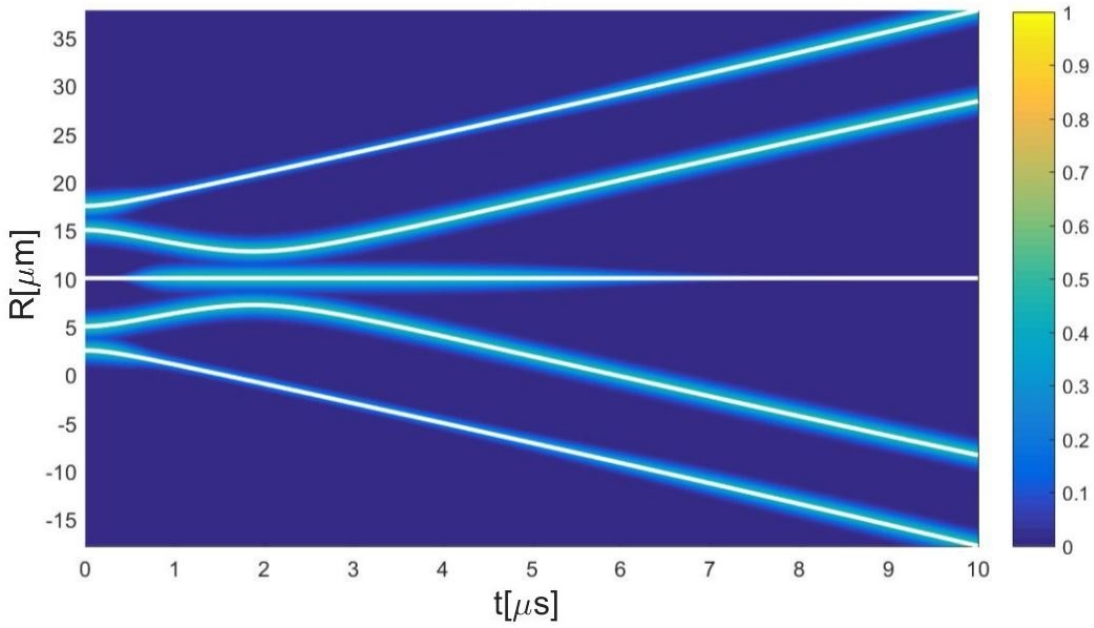


Figure 4.4: Atomic trajectories (white lines) with excitation density for the states $\zeta_{10}^5$ of a dislocated chain at two ends.

Next, we look into single trajectories of biexciton states for both a dislocated chain at two ends and a dislocated chain at one end, shown in shown in Fig. 4.5 and Fig. 4.4 respectively. The atomic trajectories are represented as white lines, along with the probability of finding an excitation on a certain atom represented by color shading according to the color-bar.

In Fig. 4.4, the system start in the initial state $\zeta_{10}^5$. Here, each excitation is localized on one end and as the system evolves in time, the excitation pulses interact in the middle and then get reflected. This an exclusive property of biexciton states as it does not happen in single excitons.

In Fig. 4.5 (a) the system initially starts in the state $\zeta_9^5$ while in 4.5 (b) it is in $\zeta_1^50$. Here, we notice that The initial states play an important role in determining the excitation dynamics through the chain. For both we have an incoming exciton-motion pulse from the dislocated atoms 1,2 sharing one p, while the second p is distributed over atoms 3-5. From Fig. 3.3 we notice that for (a), the second excitation corresponds to the state $\phi_2^3$, and for (b), the state $\phi_1^3$.

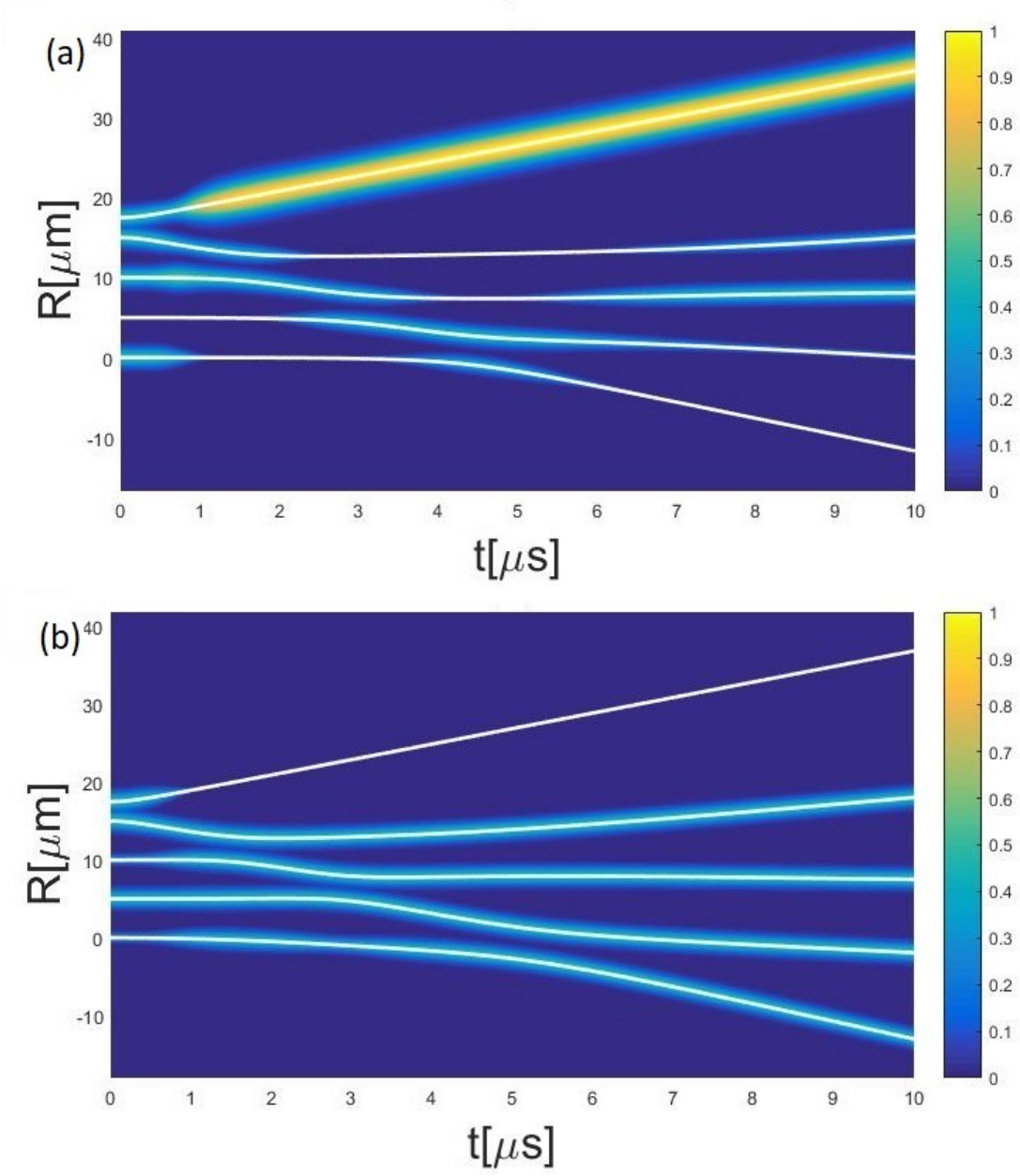


Figure 4.5: Atomic trajectories (white lines) with excitation density for the states $\zeta_9^5$ in (a) and $\zeta_{10}^5$ in (b) of a dislocated chain at one end.

By comparing both plots, we notice that they can be viewed as a transmission switch. In Fig. 4.5 (a), the excitonic pulse coming from the top two atoms gets reflected as it interacts with the pulse coming from the bottom three atoms, whereas in Fig. 4.5 (b) the pulse is transmitted.

We now move to a more sophisticated description, where we consider a system that is prepared in one of the electronic Hamiltonian eigenstates $\zeta_k^N$, where atoms are assumed to be optically trapped in a harmonic potential before they are released to freely move in one direction. This, along with the fact that the system is in an ultra-cold environment, allows us to use a Gaussian probability distribution for initial positions with a standard deviation $\sigma$ and for initial velocities with $\sigma_v = \hbar/(M\sigma)$. Thus, to account for the randomness in initial positions and velocities, a large number of propagated trajectories $N_{traj}$ needs to be sampled. A useful concept here is the total atomic density $n(x,t)$ in which the spatial coordinates are defined on a discrete grid with a total number of bins $N_{grid}$, such that

$$n(x,t) = \sum_{i=1}^{N_{traj}} \sum_{j=1}^{N} \sum_{m=1}^{N_{grid}} \Theta\Big(\frac{\Delta}{2} - |x_m - x|\Big) \times \Theta\Big(\frac{\Delta}{2} - |R_{j,x}^{(i)}(t) - x_m|\Big)/NN_{\text{traj}}, \quad (4.8)$$

where $\Theta(x)$ is the Heaviside function, $\Delta$ is the size of a bin, $R_{j,x}^{(i)}(t)$ are the coordinates of the $j$'th atom from the $i$'th trajectory and $x_m$ are the coordinates of central bins.

For a large number of trajectories, we can check whether non-adiabatic transitions between BO surfaces are correctly simulated by comparing the average of adiabatic populations with the average fraction of trajectories $f_k$ so that both statistically agree for each BO surface, where

$$f_k(t) := \frac{1}{N_{traj}} \sum_{i=1}^{N_{traj}} \delta_{k\gamma_2(t)}, \quad (4.9)$$

here $k$ is a chosen adiabatic surface and $\gamma_2(t)$ represents the adiabatic surface that the system follows as it evolves in time.

Fig. 4.6 (a) shows the total atomic density for a dislocated chain of $N = 5$, where the distance between nearest neighbors is $R = 5\mu m$ except for the last two atoms $R_{45} = 2.5\mu m$. Initially, the aggregate is prepared in the electronic state $\zeta_5^5$ and then propagated over $10^3$ trajectories with $\sigma = 0.3\mu m$. We notice that the trajectories start broadening at around $1\mu s$, which indicates that atoms are following different trajectories.

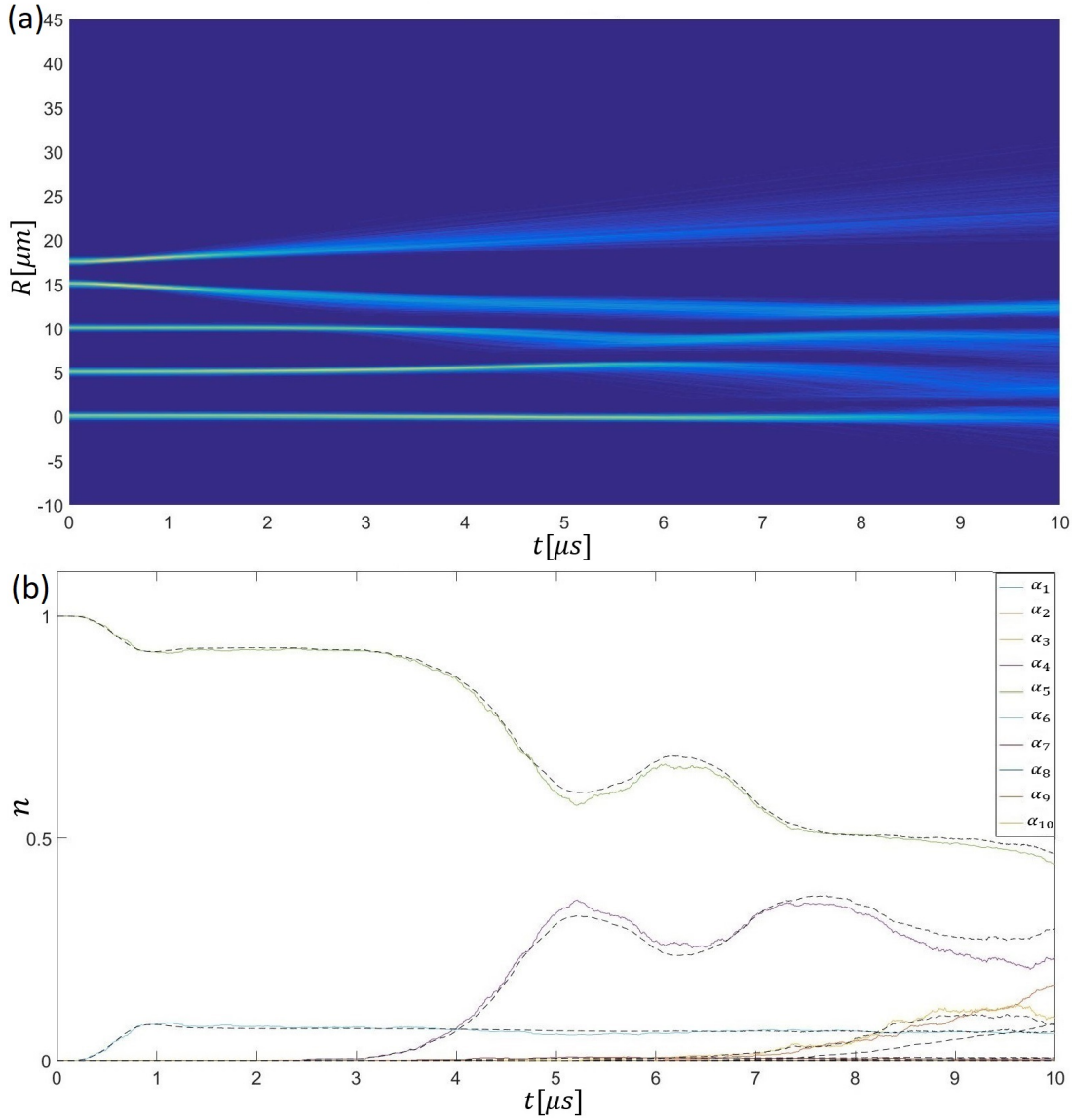


Figure 4.6: (a) Atomic density for the state $\zeta_5^5$ of a chain of 5 Rydberg atoms with two excitations. (b) the adiabatic populations $\alpha_k$ "dashed lines" and trajectory fractions "solid lines" for the same state in (a).

This can be explained by looking at Fig. 4.6 (b) where we present the adiabatic populations $\alpha_k$ (dashed lines) and trajectory fractions (solid lines) which indicate that the population is moving from $\alpha_5$ to other BO surfaces as indicated by the dips in $\alpha_5$ plot. The results clearly indicates that non-adiabatic effects are present in a one-dimensional configuration which has not been reported before.

## 4.3 Conclusion

In this chapter the dynamics of a flexible Rydberg chain has been studied. We have shown the trajectories of a chain of 5 atoms with one excitation in the chain and explained how the initial state of the system affects possible trajectories. Moreover, we presented the trajectories for a regular chain of 5 atoms that has two excitations. Next, we demonstrated that in dislocated chains, two excitation pulses interact with each other and the initial state of the system determines whether the pulses are reflected or transmitted. We have shown that for biexciton states, non-adiabatic effects play an important role in determining the dynamics and excitation transport.

# Chapter 5

# Conclusion

The topic of this thesis was to explore different aspects of multi-exciton states in a flexible Rydberg aggregate. We started with a review of single exciton states for a number of chains where atoms are confined to move in one dimension. Moreover, we showed that the direction of initial forces in the system is determined by the sign of the probability amplitudes of finding the excitation on a certain atom, consequently affecting the atomic trajectories in a repulsive or an attractive manner.

By adding a second excitation to the chain, biexciton states can be investigated. We demonstrate that for a regular chain of five atoms, both excitations will be shared among all atoms for every exciton state. However, by introducing a dislocation at one end, the distance between the last two atoms in the chain is halved. We notice that the delocalization is reduced and the excitation density is localized on a number of specific atoms. In a way, this can be represented as the product of two excitons describing two chains with one excitation on each of them.

We have also investigated the coupling between dipole-dipole interaction and atomic motion through simulating the dynamics using a mixed quantum-classical

model. Here, the electronic wavefuntion was considered in a full quantum mechanical manner, while the nuclear motion was classically simulated. We showed that, for a dislocated chain at one end, the interaction between two excitation pulses depends on the initial excitonic state. In one case, the pulse coming from the dislocation is transmitted and in the other case, the pulse is reflected. This works in a similar way to a transmission switch. Additionally, we used Tully's FSSH algorithm to account for the possibility of exciton jumps between BO surfaces. According to the obtained results, non-adiabatic crossings are indeed present in one-dimensional Rydberg aggregates.

These findings are broadly in line and follow up on previous research done by Prof. Sebastian Wüster and his colleagues at Max Planck Institute for the Physics of Complex Systems in Germany [14, 15, 22, 23, 43].

Our model can be straightforwardly generalized for any number of atoms and excitations. However, going up to higher excitations is computationally demanding, especially when propagating a large number of trajectories in the FSSH algorithm. We must also emphasize that the suggested model does not account for spin-orbit coupling which is justified by the use of $Li$ as a specimen in our numerical simulations. Therefore, in case of atoms in which spin-orbit coupling plays a significant role, the model has to be modified to include it. The modification of the model will be a focus in our future studies. Additionally, we can extend our work by studying higher dimensional configurations, mainly looking for the effects of conical intersections on exciton dynamics. Another area to be considered is a qualitative measure of entanglement and coherence in the system.

# Bibliography


[1] M. Planck, "Zur Theorie des Gesetzes der Energieverteilung im Normalspektrum," *Verhandlungen der Deutschen Physikalischen Gesellschaft*, vol. 2, no. 237, 1900.

[2] A. Einstein, "Über einen die Erzeugung und Verwandlung des Lichtes betreffenden heuristischen Gesichtspunkt," *Annalen der Physik*, vol. 322, no. 6, pp. 132–148, 1905.

[3] N. Bohr, *The theory of spectra and atomic constitution*. Cambridge At The University Press, 1922.

[4] S. Chung and C. C. Lin, "Excitation of the Electronic States of the Nitrogen Molecule by Electron Impact," *Phys. Rev. A*, vol. 6, pp. 988–1002, Sep 1972.

[5] M. Haugh, T. G. Slanger, and K. D. Bayes, "Electronic Excitation Accompanying Charge Exchange," *The Journal of Chemical Physics*, vol. 44, no. 2, pp. 837–839, 1966.

[6] T. H. Maiman, "Stimulated Optical Radiation in Ruby," *Nature*, vol. 187, pp. 493–494, Aug. 1960.

[7] D. Tong, S. M. Farooqi, J. Stanojevic, S. Krishnan, Y. P. Zhang, R. Côté, E. E. Eyler, and P. L. Gould, "Local Blockade of Rydberg Excitation in an Ultracold Gas," *Phys. Rev. Lett.*, vol. 93, p. 063001, Aug 2004.

[8] T. W. Hänsch and A. L. Schawlow, "Cooling of gases by laser radiation," *Optics Communications*, vol. 13, p. 68, Jan. 1975.

[9] W. D. Phillips, J. V. Prodan, and H. J. Metcalf, "Laser cooling and electromagnetic trapping of neutral atoms," *J. Opt. Soc. Am. B*, vol. 2, pp. 1751–1767, Nov 1985.

[10] M. D. Lukin, M. Fleischhauer, R. Côté, L. M. Duan, D. Jaksch, J. I. Cirac, and P. Zoller, "Dipole Blockade and Quantum Information Processing in Mesoscopic Atomic Ensembles," *Phys. Rev. Lett.*, vol. 87, p. 037901, Jun 2001.

[11] W. R. Anderson, J. R. Veale, and T. F. Gallagher, "Resonant Dipole-Dipole Energy Transfer in a Nearly Frozen Rydberg Gas," *Phys. Rev. Lett.*, vol. 80, pp. 249–252, Jan 1998.

[12] T. Amthor, M. Reetz-Lamour, S. Westermann, J. Denskat, and M. Weidemüller, "Mechanical Effect of van der Waals Interactions Observed in Real Time in an Ultracold Rydberg Gas," *Phys. Rev. Lett.*, vol. 98, p. 023004, Jan 2007.

[13] C. Ates, A. Eisfeld, and J. M. Rost, "Motion of Rydberg atoms induced by resonant dipole-dipole interactions," *New Journal of Physics*, vol. 10, no. 4, p. 045030, 2008.

[14] S. Möbius, S. Wüster, C. Ates, A. Eisfeld, and J. M. Rost, "Adiabatic entanglement transport in Rydberg aggregates," *Journal of Physics B: Atomic, Molecular and Optical Physics*, vol. 44, no. 18, p. 184011, 2011.

[15] S. Wüster, C. Ates, A. Eisfeld, and J. M. Rost, "Newton's Cradle and Entanglement Transport in a Flexible Rydberg Chain," *Phys. Rev. Lett.*, vol. 105, p. 053004, Jul 2010.

[16] J. Deiglmayr, M. Reetz-Lamour, T. Amthor, S. Westermann, A. de Oliveira, and M. Weidemüller, "Coherent excitation of Rydberg atoms in an ultracold gas," *Optics Communications*, vol. 264, no. 2, pp. 293 – 298, 2006. Quantum Control of Light and Matter.

[17] S. Wüster, A. Eisfeld, and J. M. Rost, "Conical Intersections in an Ultracold Gas," *Phys. Rev. Lett.*, vol. 106, p. 153002, Apr 2011.

[18] S. Sevinçli, N. Henkel, C. Ates, and T. Pohl, "Nonlocal Nonlinear Optics in Cold Rydberg Gases," *Phys. Rev. Lett.*, vol. 107, p. 153001, Oct 2011.

[19] T. Killian, T. Pattard, T. Pohl, and J. Rost, "Ultracold neutral plasmas," *Physics Reports*, vol. 449, no. 4?5, pp. 77 – 130, 2007.

[20] H. Weimer, M. Müller, I. Lesanovsky, P. Zoller, and H. P. Büchler, "A Rydberg quantum simulator," *Nat Phys*, vol. 6, pp. 382–388, May 2010.

[21] M. Saffman, T. G. Walker, and K. Mølmer, "Quantum information with Rydberg atoms," *Rev. Mod. Phys.*, vol. 82, pp. 2313–2363, Aug 2010.

[22] H. Zoubi, A. Eisfeld, and S. Wüster, "Van der Waals stabilized Rydberg aggregates," *Phys. Rev. A*, vol. 89, p. 053426, May 2014.

[23] K. Leonhardt, S. Wüster, and J. M. Rost, "Orthogonal flexible Rydberg aggregates," *Phys. Rev. A*, vol. 93, p. 022708, Feb 2016.

[24] D. W. Schönleber, A. Eisfeld, M. Genkin, S. Whitlock, and S. Wüster, "Quantum Simulation of Energy Transport with Embedded Rydberg Aggregates," *Phys. Rev. Lett.*, vol. 114, p. 123005, Mar 2015.

[25] K. Leonhardt, S. Wüster, and J. M. Rost, "Exciton induced directed motion of unconstrained atoms in an ultracold gas," *Journal of Physics B: Atomic, Molecular and Optical Physics*, vol. 50, no. 5, p. 054001, 2017.

[26] S. Wüster, "Quantum Zeno suppression of dipole-dipole forces," *arXiv:1611.07697 [quant-ph]*, 2017.

[27] J. C. Tully and R. K. Preston, "Trajectory Surface Hopping Approach to Nonadiabatic Molecular Collisions: The Reaction of H+ with D2," *The Journal of Chemical Physics*, vol. 55, no. 2, pp. 562–572, 1971.

[28] J. C. Tully, "Molecular dynamics with electronic transitions," *The Journal of Chemical Physics*, vol. 93, no. 2, pp. 1061–1071, 1990.

[29] M. Barbatti, "Nonadiabatic dynamics with trajectory surface hopping method," *Wiley Interdisciplinary Reviews: Computational Molecular Science*, vol. 1, no. 4, pp. 620–633, 2011.

[30] T. F. Gallagher, *Rydberg Atoms*. Cambridge University Press, 2005.

[31] A. Sommerfeld, *Atombau und Spektrallinien*. Friedrich Vieweg und Sohn, 1919.

[32] M. Marinescu, H. R. Sadeghpour, and A. Dalgarno, "Dispersion coefficients for alkali-metal dimers," *Phys. Rev. A*, vol. 49, pp. 982–988, Feb 1994.

[33] P. Goy, J. Liang, M. Gross, and S. Haroche, "Quantum defects and specific-isotopic-shift measurements in ns and np highly excited states of lithium: Exchange effects between Rydberg and core electrons," *Phys. Rev. A*, vol. 34, pp. 2889–2896, Oct 1986.

[34] P. Goy, J. M. Raimond, G. Vitrant, and S. Haroche, "Millimeter-wave spectroscopy in cesium Rydberg states. quantum defects, fine- and hyperfine-structure measurements," *Phys. Rev. A*, vol. 26, pp. 2733–2742, Nov 1982.

[35] C. E. Theodosiou, "Lifetimes of alkali-metal–atom Rydberg states," *Phys. Rev. A*, vol. 30, pp. 2881–2909, Dec 1984.

[36] M. J. Seaton, "The Quantum Defect Method," *Monthly Notices of the Royal Astronomical Society*, vol. 118, 1958.

[37] M. J. Seaton, "Quantum defect theory," *Reports on Progress in Physics*, vol. 46, no. 2, p. 167, 1983.

[38] C. Eckart, "The Application of Group theory to the Quantum Dynamics of Monatomic Systems," *Rev. Mod. Phys.*, vol. 2, pp. 305–380, Jul 1930.

[39] F. Robicheaux, J. V. Hernández, T. Topçu, and L. D. Noordam, "Simulation of coherent interactions between Rydberg atoms," *Phys. Rev. A*, vol. 70, p. 042703, Oct 2004.

[40] K. Singer, J. Stanojevic, M. Weidemüller, and R. Côté, "Long-range interactions between alkali Rydberg atom pairs correlated to the $n$s-$n$s, $n$p-$n$p and $n$d-$n$d asymptotes," *Journal of Physics B: Atomic, Molecular and Optical Physics*, vol. 38, no. 2, p. S295, 2005.

[41] D. Barredo, H. Labuhn, S. Ravets, T. Lahaye, A. Browaeys, and C. S. Adams, "Coherent Excitation Transfer in a Spin Chain of Three Rydberg Atoms," *Phys. Rev. Lett.*, vol. 114, p. 113002, Mar 2015.

[42] J. Frenkel, "On the Transformation of light into Heat in Solids. I," *Phys. Rev.*, vol. 37, pp. 17–44, Jan 1931.

[43] K. Leonhardt, S. Wüster, and J. M. Rost, "Switching Exciton Pulses Through Conical Intersections," *Phys. Rev. Lett.*, vol. 113, p. 223001, Nov 2014.

[44] M. Dantus and A. Zewail, "Introduction: Femtochemistry," *Chemical Reviews*, vol. 104, no. 4, pp. 1717–1718, 2004.